Universal Early Coarsening of Quenched Bose Gases

Junhong Goo,[1] Yangheon Lee,[1,2] Younghoon Lim,[1,2] Dalmin Bae,[1,2] Tenzin Rabga,[2] and Y. Shin[1,2,3,*]
[1]Department of Physics and Astronomy, Seoul National University, Seoul 08826, Korea
[2]Center for Correlated Electron Systems, Institute for Basic Science, Seoul 08826, Korea
[3]Institute of Applied Physics, Seoul National University, Seoul 08826, Korea

(Received 10 December 2021; accepted 17 March 2022; published 1 April 2022)

We investigate the early coarsening dynamics of an atomic Bose gas quenched into a superfluid phase. Using a two-step quench protocol, we independently control the two cooling rates during and after passing through the critical region, respectively, and measure the number of quantum vortices spontaneously created in the system. The latter cooling rate regulates the temperature during the condensate growth, consequently controlling the early coarsening dynamics in the defect formation. We find that the defect number shows a scaling behavior with the latter cooling rate regardless of the initial cooling rate, indicating universal coarsening dynamics in the early stage of condensate growth. Our results demonstrate that early coarsening not only reduces the defect density, but also affects its scaling with the quench rate, which is beyond the Kibble-Zurek mechanism.

DOI: 10.1103/PhysRevLett.128.135701

When a system crosses a symmetry-breaking phase transition, topological defects can be spontaneously created. This defect formation originates from the causal independence of distant regions and is a generic process in nonequilibrium phase transition dynamics, which gives it broad relevance in condensed matter physics as well as cosmology [1–4]. A practically important problem is the quantitative estimation of the created defect density. However, this is a challenging problem that requires a full description of the complex phase transition dynamics, including the emergence and coarsening of the order parameter and subsequent defect formation and relaxation.

The Kibble-Zurek mechanism (KZM) provides a general framework for defect density estimation [2–4], where the system's correlation length ξ, after passing through the critical region, is assessed for a given quench rate using the system's equilibrium properties near the critical point [5] and assumed to determine the characteristic length scale of the spatial domains of the symmetry-broken phase and, consequently, the defect density. The relationship between the defect density and the quench rate was predicted to follow a universal power law and has been tested by many experiments [6–24]. Nevertheless, the Kibble-Zurek (KZ) theory inherently lacks the ability to quantitatively predict the average value of defect density, because it omits the defect formation dynamics after the freeze-out period in the critical region [25–28].

In order to produce well-defined topological defects, the order parameter must grow sufficiently, and during the growth period, the spatial fluctuations of the order parameter is inevitably coarsened, affecting the defect formation probability. We refer to this coarsening as *early* coarsening, distinguished from the coarsening at later times, where defects decay as the system relaxes to an equilibrium state (Fig. 1). Some theoretical studies have shown that the early coarsening, along with possible coarsening within the critical region [25], simply gives a logarithmic correction to the defect density [3,29]; but it was recently asserted that it can be sufficient enough to cause defect density saturation for fast enough quenches [28]. Such defect density saturation was observed in ultracold atomic gas

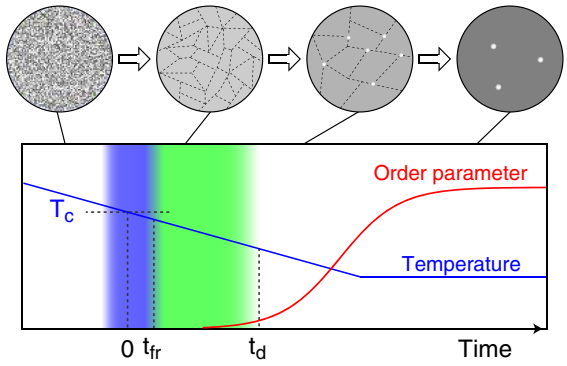

FIG. 1. Early coarsening in a quenched Bose gas. As a thermal Bose gas is cooled into a superfluid phase, it experiences an early coarsening period (green), after passing through the critical region (blue) but before the order parameter has grown significantly ($t_{fr} < t < t_d$), during which the spatial fluctuations of the system are coarsened, reducing the defect creation probability. T_c denotes the critical temperature. In the critical region, the system's dynamics is effectively frozen due to the divergence of its relaxation time at the critical point. In the upper row, the system's quench evolution is illustrated, where the boundaries of spatial domains of the symmetry-broken phase are indicated by dashed lines and quantum vortices are denoted by the white circles.

experiments [21–24], and, furthermore, its possible association with the early coarsening dynamics was demonstrated, ruling out the alternative explanation relying on rapid annihilation of defects due to their high density [23].

In this Letter, we present a direct observation of the early coarsening effect in spontaneous defect formation in a thermally quenched atomic Bose gas. We use a two-step quench protocol, where the sample is successively cooled with two different quench rates so that the temperature change during and after passing through the critical region can be effectively controlled separately. We observe that the mean number of created quantum vortices is reduced as the latter quench rate decreases, and, surprisingly, the suppression factor is independent of the initial quench rate, indicating the existence of universal early coarsening dynamics in the quenched system. Our results clearly demonstrate the early coarsening effect in spontaneous defect formation and provide a deeper perspective on the universal scaling of the defect density with quench rate, beyond the original KZM.

Our experiment starts by preparing a cold thermal ^{87}Rb gas in an optical dipole trap (ODT) with a highly oblate and elongated geometry [23,30]. The initial sample contains $\approx 3.3 \times 10^7$ atoms at a temperature of $\approx$480 nK. Then, the sample is evaporatively cooled by lowering the ODT depth U from $U_i = 1.15U_c$ to $U_m = 0.8U_c$ and successively to $U_f = 0.27U_c$ in a piecewise linear manner. Here, U_c is the critical trap depth for Bose-Einstein condensation, determined for an equilibrium sample, where the atom number is measured to be $\approx 3.0 \times 10^7$. At the end of the quench, the typical atom number is $\approx 1.2 \times 10^7$, and the sample temperature is $\approx$50 nK. In equilibrium, the condensate fraction is about 80%, and the Thomas-Fermi radii are $R_{x,y,z} \approx (65, 244, 2.8)$ μm. After the quench, a hold time of $\tau_h = 1.25$ s is applied to facilitate defect formation [23], and the created vortices are detected by imaging the sample after a time of flight of 40.4 ms. The linear relationship between the sample temperature and the trap depth was confirmed for the whole range of our quench parameters, as described in Ref. [23], ensuring that the sample is sufficiently thermalized during the quench evolution. The elastic collision time of atoms is estimated to be $\approx$1 ms for the peak atom density at the critical point.

Figure 2(a) shows a schematic of the two-step quench protocol. The two cooling steps proceed with variable time durations τ_1 and τ_2, giving the quench rates $r_1 = [(U_i - U_m)/U_c] \times (1/\tau_1)$ and $r_2 = [(U_m - U_f)/U_c] \times (1/\tau_2)$, respectively. In our experiment, $r_{1(2)}$ varies from $r_m = 0.08$ s^{-1} to $r_M = 1.17$ s^{-1}, and the intermediate trap depth $U_m = 0.8U_c$ is chosen such that the sample has a negligible condensate fraction (< a few percent) immediately after the first cooling step [31]. This ensures that the condensate growth mostly occurs in the second quench period, and, thus, we can modulate the early coarsening dynamics with the variable quench rate r_2. According to previous ^{87}Rb

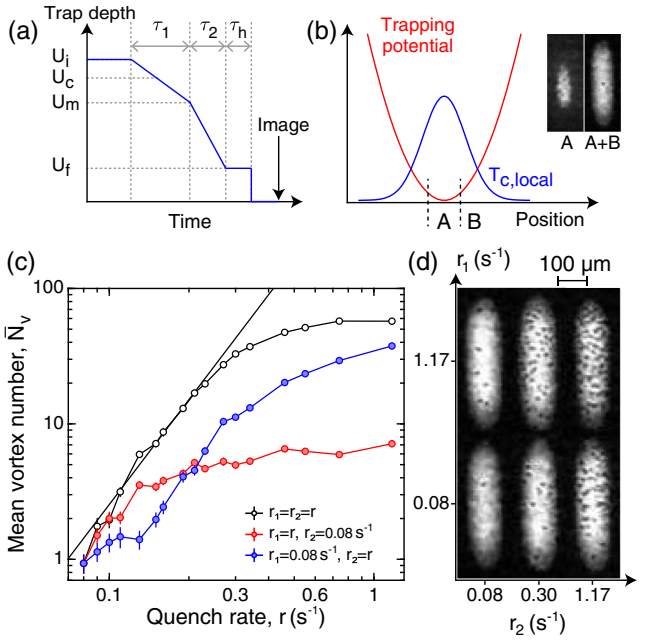

FIG. 2. Two-step quench experiment. (a) Schematic of the quench protocol. The trap depth U is linearly lowered from U_i to U_m for time τ_1 with rate r_1 and from U_m to U_f for τ_2 with rate r_2. U_c denotes the critical trap depth for Bose-Einstein condensation. After a hold time τ_h, a time-of-flight image is taken to detect created vortices. (b) For a trapped sample, the local critical temperature $T_{c,\mathrm{local}}$ spatially varies over the sample. The inner (outer) region A (B) undergoes a phase transition for $U > U_m (< U_m)$. The inset shows images of samples in equilibrium at $U = U_m$ (left) and $U = U_f$ (right). (c) Mean vortex number $\bar{N}_v$ as a function of the quench rate on log-log axes. Open circles denote the data obtained with $r_1 = r_2$, and red (blue) solid circles show the data for fixed $r_2(r_1) = 0.08$ s^{-1}. The solid line shows a power-law function with exponent $\alpha_{\mathrm{KZ}} = 2.6$, fit to the data with $r_1 = r_2$ in the scaling regime. Each data point in the blue and red (black) curves was obtained from 30 (20) realizations of the same experiment. The error bars indicate the standard errors of the mean. If the error bars are invisible, they are smaller than the marker size. (d) Representative images of samples for various r_1 and r_2, displaying quantum vortices by their expanded, density-depleted cores.

experiments [19], the unfreeze time t_{fr}, which is the time required to pass the critical region (Fig. 1), is estimated to be $\approx$55 ms ($\ll \tau_1$) for our fastest quench [32], and it is reasonable to assume that the initial seed structure of ordered-phase domains is implanted at the end of the first quench step.

In the two-step quench experiment, the early coarsening dynamics can be directly investigated by the dependence of the vortex number N_v on r_2. However, in the analysis of N_v, the density inhomogeneity of the trapped sample must be considered [33,34]. The local critical temperature $T_{c,\mathrm{local}}$ varies over the sample, which is higher in the high-density central region than in the low-density outer region [Fig. 2(b)], so the phase transition occurs at different times

in different regions of the sample during the quench. For the two-step quench, we can divide the sample into two distinct regions: the central region A, where the local phase transition occurs for $U > U_m$, i.e., the first quench period, while for the outer region B, it occurs during the second quench period with $U < U_m$. Figure 2(b) shows two time-of-flight images of the sample in equilibrium at $U = U_m$ and $U = U_f$, indicating that the area of region A is ≈36% of the final sample area. In view of the local density approximation, we model the total vortex number N_v as a sum of two contributions:

$$N_v = N_A(r_1, r_2) + N_B(r_2), \tag{1}$$

where N_A and N_B represent the numbers of vortices created in regions A and B, respectively. Note that N_B is assumed to be determined only by r_2, because region B remains thermal with $T > T_{c,\mathrm{local}}$ during the first quench period. In the following, we analyze our measurement results based on this model.

In Fig. 2(c), we display the mean vortex number $\bar{N}_v$ as a function of the quench rate for three representative cases: (I) $r_1 = r_2$, (II) $r_2 = r_m$, and (III) $r_1 = r_m$. Setting $r_1 = r_2$ corresponds to a typical single-step quench, and, as observed in Ref. [23], $\bar{N}_v$ exhibits power-law scaling for slow quench rates and saturates for quench rates over 0.3 s^{-1}. We obtain the power-law exponent $\alpha_{\mathrm{KZ}} = 2.6(1)$ from a fit to the data in the scaling regime, which is determined from a saturation model fit to the $\bar{N}_v$ curve [31]. The value of α_{KZ} is slightly smaller than our previous measurement [23], which is due to the refinement of our trap center control during the quench [31].

When r_2 is fixed at the slowest value r_m (case II), $\bar{N}_v$ initially follows the single-step quench curve but quickly becomes saturated. Since $N_B(r_m) < N_v(r_m, r_m) \approx 1$, the measured $\bar{N}_v$ can be assumed to mainly reflect $N_A(r_1, r_m)$, the vortex number of region A. In comparison with the single-step quench case, the defect saturation occurs at a lower r_1, which is accounted for by the condensate fraction being negligible at the end of the first quench step in the experiment. For the fastest $r_1 = r_M$, the maximum vortex number is $\bar{N}_{v,\mathrm{max}} < 10$, and its ratio to $\bar{N}_{v,\mathrm{max}} \approx 60$ in the single-step quench case is almost 2 times smaller than the area ratio $\eta \approx 0.36$ of region A to the whole sample. This means that $N_A(r_M, r_m) < \eta N_v(r_M, r_M) < N_A(r_M, r_M)$, indicating the early coarsening dynamics. The second inequality results from the fact that the central region has a higher defect formation probability than the outer region.

In case III with $r_1 = r_m$, the mean vortex number is also reduced compared to the single-step quench, which is due to the suppression of defect formation in region A. It is notable that the increasing rate of $\bar{N}_v$ becomes faster as r_2 increases over 0.13 s^{-1}. This is caused by a rapid increase in N_B with increasing r_2, and we infer that $N_B > N_A$ for $r_2 > 0.13$ s^{-1}; i.e., there are more vortices in the outer region than in the central region.

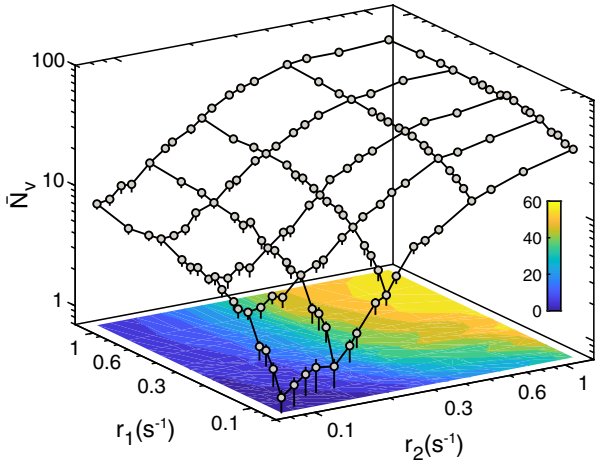

FIG. 3. Mean vortex number $\bar{N}_v$ as a function of r_1 and r_2 on three-dimensional log axes. Each data point was obtained from 20 realizations of the same experiment, except one with $r_{1(2)} = r_m$ which was obtained from 30 measurements [the same data in Fig. 2(c)]. The error bars indicate the standard errors of the mean.

To investigate the early coarsening effect in a systematic manner, we measure $\bar{N}_v$ by scanning over a range of values of r_1 and r_2. The measurement results are displayed in Fig. 3. As expected from the results as shown in Fig. 2(c), $\bar{N}_v$ monotonically increases with both r_1 and r_2 and saturates at fast quench rates. To isolate the contribution of N_A to $\bar{N}_v$, we consider the following quantity:

$$\begin{aligned}\mathcal{D}(r_1, r_2) &= \bar{N}_v(r_1, r_2) - \bar{N}_v(r_m, r_2) \\ &= N_A(r_1, r_2) - N_A(r_m, r_2).\end{aligned} \tag{2}$$

For a given value of r_2, this quantifies the increase in $\bar{N}_v$ as r_1 increases from r_m. Therefore, the r_2 dependence of $\mathcal{D}$ should unambiguously reveal the early coarsening effect in the defect formation process.

In Fig. 4(a), we plot $\mathcal{D}$ as a function of r_2 for various r_1. We observe that, regardless of the value of r_1, $\mathcal{D}$ increases over the range of $r_2 < 0.5$ s^{-1}. This is consistent with the effect of early coarsening; i.e., with a slower second quench at a small r_2, the system stays at a high temperature for longer such that the condensate grows slowly, allowing more time for the coarsening of the spatial fluctuations before defects are stably formed, thus reducing the final defect number.

Meanwhile, the different plots in Fig. 4(a) show similar profiles for all values of r_1. In Fig. 4(b), we replot the four data curves by multiplying each curve by a scaling factor to give the same average value for the four slowest r_2. Remarkably, we find that the four scaled curves overlap. This indicates the existence of a universal curve $f(\tilde{r}_2)$ that satisfies the factorization of $\mathcal{D} = f(\tilde{r}_2)\mathcal{D}(r_1, r_m)$ with

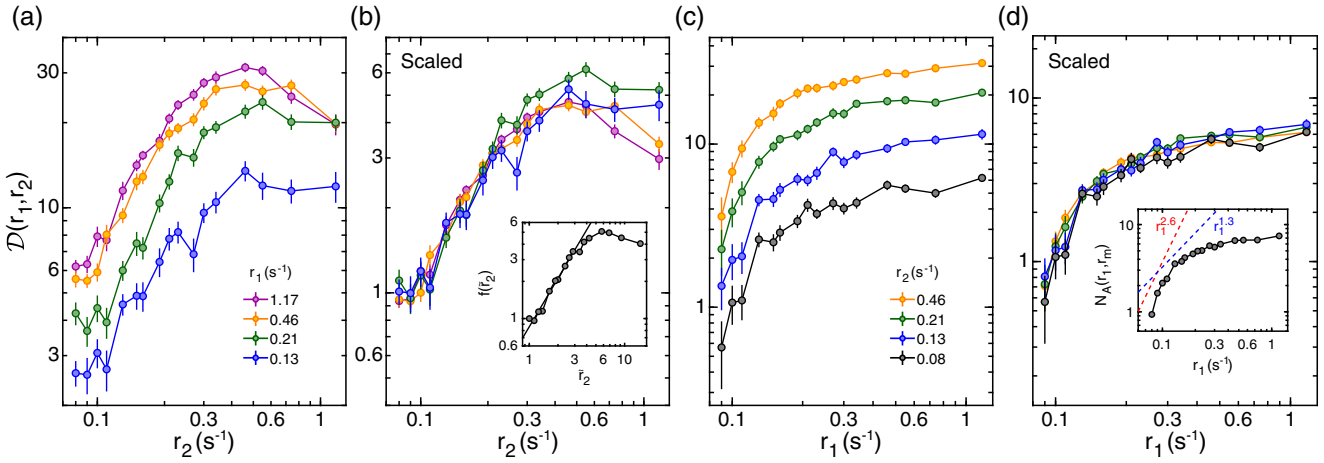

FIG. 4. Universal scaling of early coarsening. For a given value of r_2, $\mathcal{D}(r_1, r_2)$ denotes the increase in $\bar{N}_v$ as r_1 increases from r_m [Eq. (2)]. (a) $\mathcal{D}$ as functions of r_2 for four different r_1 on log-log axes and (b) the same curves after scaling (see the text for details). The inset in (b) presents a universal curve $f(\tilde{r}_2)$ ($\tilde{r}_2 = r_2/r_m$) obtained from averaging the data in (b), and the solid line shows a power-law function with exponent $\beta = 1.3$, fit to the data in the scaling regime ($\tilde{r}_2 < 2.5$). (c) $\mathcal{D}$ as functions of r_1 for four different r_2 on log-log axes and (d) the same curves after divided by $f(\tilde{r}_2)$. The inset in (d) presents $N_A(r_1, r_m)$ calculated from the data in (d) (see the text for details), and the dashed lines are power-law guide lines. The error bars in (a)–(d) are the standard errors of the measured quantities.

$\tilde{r}_2 = r_2/r_m$. To corroborate this factorization, we plot $\mathcal{D}$ as a function of r_1 for four different values of r_2 in Fig. 4(c). As can be seen in Fig. 4(d), the four curves overlap after being divided by $f(\tilde{r}_2)$, where the value of $f(\tilde{r}_2)$ was determined by averaging the four curves in Fig. 4(b). The curve overlaps observed in Figs. 4(b) and 4(d) lead us to suggest the following relation:

$$N_A(r_1, r_2) = f(\tilde{r}_2) N_A(r_1, r_m), \tag{3}$$

where $f(\tilde{r}_2)$ represents the suppression factor accounting for the universal coarsening dynamics in the early stage of defect formation. This finding is the main result of this work.

The profile of $f(\tilde{r}_2)$ provides more information on the early coarsening effect. Similar to $\bar{N}_v$ in the single-step quench case, it shows a power-law-like behavior for low r_2 and becomes saturated for high $r_2 > 0.3\ \mathrm{s}^{-1}$. This is consistent with the postquench condensate growth observed for high r_2 [31]. From a power-law function fit to the data in the scaling regime $r_2 \lesssim 0.2$, determined using a saturation model curve as in the single-step quench case [31], we obtain a scaling exponent of $\beta = 1.3(2)$ [Fig. 4(b), inset]. It is surprising that the measured value is large, approximately half the Kibble-Zurek exponent of $\alpha_{\mathrm{KZ}} = 2.6(1)$ in the single-step quench experiment [Fig. 1(c)]. In previous studies, α_{KZ} has been associated only with how fast the system passes through the critical region, i.e., the *seeding* process, neglecting the early coarsening dynamics. Our observation of large β challenges the conventional interpretation of α_{KZ} based on the KZ theory, demonstrating the significance of the early coarsening dynamics in the defect formation.

An important follow-up question is whether the difference between the two exponents, $\alpha_{\mathrm{KZ}} - \beta \approx 1.3$, can represent the scaling exponent for the KZ seeding process. Currently, we have no clear answer to the question. In the inset in Fig. 4(d), we display $N_A(r_1, r_m)$ as a function of r_1, which, as shown in Eq. (3), is the number of vortices in region A after scaling it by the coarsening factor $f(\tilde{r}_2)$. From Eqs. (2) and (3), $N_A(r_1, r_m) = \mathcal{D}/f(\tilde{r}_2) + N_A(r_m, r_m)$, and we calculate this by determining $\mathcal{D}/f$ by averaging the data in Fig. 4(d) and assuming $N_A(r_m, r_m) = \bar{N}_v(r_m, r_m)$. A clear power-law behavior is not observed. It should be noted that our analysis is based on the two-region model that ignores possible physics at the regional interface in the inhomogeneous system, such as phase information propagation that would suppress defect formation [33,34]. Further theoretical and experimental investigations are warranted. Similar two-step quench experiments with homogeneous samples [19,20], in particular, correlating the defect density with the correlation length ξ [19], would be fruitful to reveal the details of the universal early coarsening dynamics.

In summary, we have investigated the early coarsening in a quenched atomic Bose gas. The two-step quench protocol was introduced to effectively control the coarsening dynamics during spontaneous defect formation, and the defect number in the central region of the sample was found to be factorizable into functions of each quench rate. Our results demonstrate the existence and characteristics of early coarsening, highlighting the condensate growth dynamics after passing through the critical region. We anticipate that the early coarsening dynamics of the quenched system could be further studied in light of the physics of nonthermal fixed points [35,36], which considers the universal scaling of the

spatiotemporal evolution of quantum many-body systems far from equilibrium.

This work was supported by the National Research Foundation of Korea (NRF-2018R1A2B3003373 and NRF-2019M3E4A1080400) and the Institute for Basic Science in Korea (IBS-R009-D1).

*yishin@snu.ac.kr

[1] T. W. B. Kibble, Topology of cosmic domains and strings, J. Phys. A **9**, 1387 (1976).
[2] W. H. Zurek, Cosmological experiments in superfluid helium?, Nature (London) **317**, 505 (1985).
[3] W. H. Zurek, Cosmological experiments in condensed matter systems, Phys. Rep. **276**, 177 (1996).
[4] J. Dziarmaga, Dynamics of a quantum phase transition and relaxation to a steady state, Adv. Phys. **59**, 1063 (2010).
[5] P. C. Hohenberg and B. I. Halperin, Theory of dynamic critical phenomena, Rev. Mod. Phys. **49**, 435 (1977).
[6] P. C. Hendry, N. S. Lawson, R. A. M. Lee, P. V. E. McClintock, and C. D. H. Williams, Generation of defects in superfluid ^{4}He as an analogue of the formation of cosmic strings, Nature (London) **368**, 315 (1994).
[7] C. Bäuerle, Y. M. Bunkov, S. N. Fisher, H. Godfrin, and G. R. Pickett, Laboratory simulation of cosmic string formation in the early Universe using superfluid ^{3}He, Nature (London) **382**, 332 (1996).
[8] V. M. H. Ruutu, V. B. Eltsov, A. J. Gill, T. W. B. Kibble, M. Krusius, Yu. G. Makhlin, B. Plaçais, G. E. Volovik, and Wen Xu, Vortex formation in neutron-irradiated superfluid ^{3}He as an analogue of cosmological defect formation, Nature (London) **382**, 334 (1996).
[9] I. Chuang, R. Durrer, N. Turok, and B. Yurke, Cosmology in the laboratory: Defect dynamics in liquid crystals, Science **251**, 1336 (1991).
[10] R. Carmi, E. Polturak, and G. Koren, Observation of Spontaneous Flux Generation in a Multi-Josephson-Junction Loop, Phys. Rev. Lett. **84**, 4966 (2000).
[11] R. Monaco, J. Mygind, and R. J. Rivers, Zurek–Kibble Domain Structures: The Dynamics of Spontaneous Vortex Formation in Annular Josephson Tunnel Junctions, Phys. Rev. Lett. **89**, 080603 (2002).
[12] K. Pyka, J. Keller, H. L. Partner, R. Nigmatullin, T. Burgermeister, D. M. Meier, K. Kuhlmann, A. Retzker, M. B. Plenio, W. H. Zurek, A. del Campo, and T. E. Mehlstäubler, Topological defect formation and spontaneous symmetry breaking in ion Coulomb crystals, Nat. Commun. **4**, 2291 (2013).
[13] S. Ulm, J. Roßnagel, G. Jacob, C. Degünther, S. T. Dawkins, U. G. Poschinger, R. Nigmatullin, A. Retzker, M. B. Plenio, F. Schmidt-Kaler, and K. Singer, Observation of the Kibble–Zurek scaling law for defect formation in ion crystals, Nat. Commun. **4**, 2290 (2013).
[14] S. Ejtemaee and P. C. Haljan, Spontaneous nucleation and dynamics of kink defects in zigzag arrays of trapped ions, Phys. Rev. A **87**, 051401(R) (2013).
[15] L. E. Sadler, J. M. Higbie, S. R. Leslie, M. Vengalattore, and D. M. Stamper-Kurn, Spontaneous symmetry breaking in a quenched ferromagnetic spinor Bose–Einstein condensate, Nature (London) **443**, 312 (2006).
[16] C. N. Weiler, T. W. Neely, D. R. Scherer, A. S. Bradley, M. J. Davis, and B. P. Anderson, Spontaneous vortices in the formation of Bose–Einstein condensates, Nature (London) **455**, 948 (2008).
[17] G. Lamporesi, S. Donadello, S. Serafini, F. Dalfovo, and G. Ferrari, Spontaneous creation of Kibble–Zurek solitons in a Bose–Einstein condensate, Nat. Phys. **9**, 656 (2013).
[18] L. Corman, L. Chomaz, T. Bienaimé, R. Desbuquois, C. Weitenberg, S. Nascimbène, J. Dalibard, and J. Beugnon, Quench-Induced Supercurrents in an Annular Bose Gas, Phys. Rev. Lett. **113**, 135302 (2014).
[19] N. Navon, A. L. Gaunt, R. P. Smith, and Z. Hadzibabic, Critical dynamics of spontaneous symmetry breaking in a homogeneous Bose gas, Science **347**, 167 (2015).
[20] L. Chomaz, L. Corman, T. Bienaimé, R. Desbuquois, C. Weitenberg, S. Nascimbène, J. Beugnon, and J. Dalibard, Emergence of coherence via transverse condensation in a uniform quasi-two-dimensional Bose gas, Nat. Commun. **6**, 6162 (2015).
[21] S. Donadello, S. Serafini, T. Bienaimé, F. Dalfovo, G. Lamporesi, and G. Ferrari, Creation and counting of defects in a temperature-quenched Bose–Einstein condensate, Phys. Rev. A **94**, 023628 (2016).
[22] B. Ko, J. W. Park, and Y. Shin, Kibble–Zurek universality in a strongly interacting Fermi superfluid, Nat. Phys. **15**, 1227 (2019).
[23] J. Goo, Y. Lim, and Y. Shin, Defect Saturation in a Rapidly Quenched Bose Gas, Phys. Rev. Lett. **127**, 115701 (2021).
[24] X.-P. Liu, X.-C. Yao, Y. Deng, Y.-X. Wang, X.-Q. Wang, X. Li, Q. Chen, Y.-A. Chen, and J.-W. Pan, Dynamic formation of quasicondensate and spontaneous vortices in a strongly interacting Fermi gas, Phys. Rev. Research **3**, 043115 (2021).
[25] G. Biroli, L. Cugliandolo, and A. Sicilia, Kibble–Zurek mechanism and infinitely slow annealing through critical points, Phys. Rev. E **81**, 050101(R) (2010).
[26] A. Chandran, F. J. Burnell, V. Khemani, and S. L. Sondhi, Kibble–Zurek scaling and string-net coarsening in topologically ordered systems, J. Phys. Condens. Matter **25**, 404214 (2013).
[27] P. Gagel, P. P. Orth, and J. Schmalian, Universal postquench coarsening and aging at a quantum critical point, Phys. Rev. B **92**, 115121 (2015).
[28] P. M. Chesler, A. M. García-García, and H. Liu, Defect Formation beyond Kibble–Zurek Mechanism and Holography, Phys. Rev. X **5**, 021015 (2015).
[29] A. Das, J. Sabbatini, and W. H. Zurek, Winding up superfluid in a torus via Bose–Einstein condensation, Sci. Rep. **2**, 352 (2012).
[30] Y. Lim, J. Goo, H. Kwak, and Y. Shin, Large-area ^{87}Rb Bose–Einstein condensate in a clipped-Gaussian optical dipole trap, Phys. Rev. A **103**, 063319 (2021).
[31] See Supplemental Material at http://link.aps.org/supplemental/10.1103/PhysRevLett.128.135701 for experimental data on the condensate growth dynamics, estimation of N_B, and details of scaling exponent determination and trap center control.
[32] According to the results in Ref. [19], $t_{\mathrm{fr}} \approx 1.9\sqrt{\tau_Q \tau_{\mathrm{el}}}$, where $\tau_Q^{-1} = -(1/T_c)(dT/dt)$ and τ_{el} is the elastic scattering time.

In our experiment, $\tau_{\mathrm{el}} \approx 1$ ms for the peak atom density at the critical point, and we estimate $t_{\mathrm{fr}} \approx 55$ ms for $\tau_Q = r_M^{-1} = 0.85$ s.

[33] A. del Campo, A. Retzker, and M. B. Plenio, The inhomogeneous Kibble–Zurek mechanism: Vortex nucleation during Bose–Einstein condensation, New J. Phys. **13**, 083022 (2011).

[34] A. del Campo, T. W. B. Kibble, and W. H. Zurek, Causality and non equilibrium second-order phase transitions in inhomogeneous systems, J. Phys. Condens. Matter **25**, 404210 (2013).

[35] J. Berges, A. Rothkopf, and J. Schmidt, Nonthermal Fixed Points: Effective Weak Coupling for Strongly Correlated Systems Far from Equilibrium, Phys. Rev. Lett. **101**, 041603 (2008).

[36] B. Nowak, D. Sexty, and T. Gasenzer, Superfluid turbulence: Nonthermal fixed point in an ultracold Bose gas, Phys. Rev. B **84**, 020506(R) (2011).